Tetrahedron 64 (2008) 8504–8514

Contents lists available at ScienceDirect

Tetrahedron

journal homepage: www.elsevier.com/locate/tet

Self-assembly of amphiphiles with terthiophene and tripeptide segments into helical nanostructures

Wei-Wen Tsai [a], Liang-shi Li [a], Honggang Cui [b], Hongzhou Jiang [b], Samuel I. Stupp [a,b,c,*]

[a] Department of Chemistry, Northwestern University, Evanston, IL 60208-3113, USA
[b] Department of Materials Science and Engineering, Northwestern University, Evanston, IL 60208-3113, USA
[c] Department of Medicine, Northwestern University, Evanston, IL 60208-3113, USA

ARTICLE INFO

Article history:
Received 16 April 2008
Received in revised form 6 June 2008
Accepted 11 June 2008
Available online 13 June 2008

Keywords:
Self-assembly
Helical nanostructure
Stereochemistry
Terthiophene

ABSTRACT

We previously reported a class of tripeptide amphiphiles known as peptide lipids that self-assemble into one-dimensional nanostructures with superhelical twisting. The pitch of this supramolecular twisting is controlled directly through sterics in the molecular structure of hydrophobic segments. In this work we study the supramolecular behavior of these nanoscale helices by substituting with a terthiophene conjugated segment of potential electronic interest and also through variations in the stereochemistry of the tripeptide. This terthiophene peptide lipid was shown to self-assemble into one-dimensional helical nanofibers with a regular diameter of 9±1 nm and helical pitch of 65±6 nm, and also found to form hierarchical double- and triple-stranded helices, which could be associated with terthiophene J-aggregate interactions among fibers. For stereochemical effects, we compared four diastereomers in the tripeptide sequence using L-glutamic acid and L- and D-alanine residues to probe their ability to control supramolecular organization. Interestingly, we found by atomic force microscopy that the LLD diastereomers formed cylindrical nanofibers without any twisting, whereas LDD diastereomeric segments self-assembled into helical nanofibers with a pitch of 40±6 nm. LDL diastereomeric segments formed, on the other hand, aggregates without any regular shape. We propose that these profound effects of chirality with amino acid sequence are related to changes in the β-sheet sub-structure within the nanofibers.

1. Introduction

Supramolecular self-assembly is the spontaneous process of molecular aggregation into ordered nanostructures and provides a bottom-up approach to obtain structural regularity of various morphologies.[1] Helical nanostructures have received attention because of their potential applications in nanoelectromechanical systems (NEMS) as nanosprings, nanoactuators, or nanosensors.[2] Supramolecular nanohelices including fibers,[3] ribbons,[4] or tubes[5] have been constructed by different strategies from organic materials. In nature, helices are essential structural elements in both DNA and protein secondary structures. The self-assembly of polypeptides sometimes leads to the formation of pathological, β-sheet-rich helical protein filaments known as amyloids associated with diseases such as Alzheimer's or type 2 diabetes.[6] It is well-established that within a β-sheet structure, adjacent β-strands stack in a right-hand-twisted conformation, which usually results in helical fibrils with a left-handed sense (called β-helices).[7] An X-ray diffraction model of amyloid fibrils clearly revealed the structure of a protofilament in which several β-sheets stacked parallelly to the fiber axis with the component β-strands extended perpendicularly to the axis.[8] Inspired by these natural systems, one-dimensional peptidic supramolecular structures have been synthesized for biological applications[9] and the sequence-dependent self-assembly mechanisms have been extensively investigated.[10] The hydrogen bonding of amino acids, in some cases, promotes the formation of a supramolecular helical nanostructure.[11]

Controlling helical architectures involves structural parameters such as size, pitch, or helical sense.[12] We reported previously a system in which the pitch of a supramolecular helical nanofiber can be tuned by chemical modification of monomers.[3a] Yamada et al. developed a class of peptide lipids (PL, Fig. 1a) in which the tripeptide segments formed β-sheets resulting in the formation of straight cylindrical nanofibers in nonpolar organic solvents.[13] Figure 1b illustrates the proposed model of a self-assembled nanofiber in which the hydrophilic ammonium bromides are

* Corresponding author. Northwestern University, Board of Trustees Professor of Materials Science, Chemistry, and Medicine, Director of the Institute for BioNanotechnology in Medicine, Department of Chemistry, Cook Hall, Room 1127, 2220 Campus Drive, Evanston, IL 60208, United States. Tel.: +1 847 491 3002; fax: +1 847 491 3010.
E-mail address: s-stupp@northwestern.edu (S.I. Stupp).

0040-4020/$ – see front matter © 2008 Elsevier Ltd. All rights reserved.
doi:10.1016/j.tet.2008.06.033

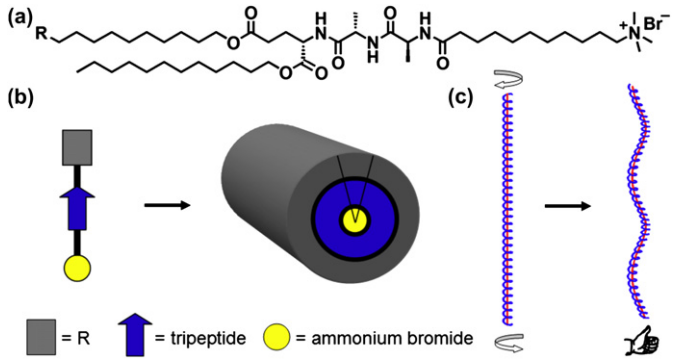

Figure 1. (a) Molecular structure of a peptide lipid. (b) Schematic representation of the self-assembly structure of a peptide lipid containing an R group of different substituents (gray square), a tripeptide (blue arrow) and an ammonium bromide (yellow circle). (c) Schematic representation of a torsional twisting of the helical nanofibers, which results in the formation of a left-handed superhelix.

located in the core and the hydrophobic alkyl tails are at the periphery in organic solvents. More recently, we found that substituting these molecules with bulky endgroups resulted in supramolecular left-handed helical nanofibers of uniform pitch. The observed helical pitch of the nanostructure has a strong correlation with the van der Waals volume of the endgroup, that is, a larger substituent leads to nanofibers with a smaller helical pitch. Since the β-sheet in the self-assembled PL nanofibers provides an intrinsically chiral primary β-helix (Fig. 1c, blue coil), we proposed that the steric repulsions of the bulky groups introduce a torsional strain within the nanofibers. To relax the strain, the elastic straight nanofibers coil with a left-handed sense into superhelices (Fig. 1c, right).

To further understand the different interactions involved in the self-assembly mechanism and superhelical twisting, we investigate here the effect of substituting the monomers with a conjugated segment as well as the role of tripeptide stereochemistry. First, a peptide lipid molecule was prepared with a terthiophene endgroup to introduce π–π interactions among the molecules. Oligothiophenes are well known for their excellent π–π stacking tendency and the ability of providing a conductive pathway for charge transport. Self-assembly of oligothiophene derivatives into one-dimensional nanostructures has been reported utilizing different strategies.[14–16] In a bis(urea)-substituted bithiophene or terthiophene system reported by Feringa et al., the extensive hydrogen bondings promote the formation of ribbon nanostructures.[16] Our group has also reported a dendron-rod-coil quarterthiophene molecule that self-assembles into nanoribbons.[4c] One-dimensional nanostructures of oligothiophenes have rarely been seen in a peptide β-sheet containing system. The substitution of a terthiophene on the PL backbone can give us insight into how the π–π interaction affects the balance of intermolecular forces that lead to self-assembled helical nanostructures. Secondly, the role of the primary β-helix in forming PL superhelices was also investigated by varying the chirality of the tripeptide segment. We report here the synthesis of four different diastereomeric PL molecules and their effect on nanostructure formation.

2. Results and discussion

2.1. Synthesis

The hydroxyl group of 11-bromo-1-undecanol was protected by tetrahydropyranyl to generate compound **1** (Scheme 1).[3a] Compound **2** was synthesized by treating terthiophene with *n*-butyllithium at −78 °C for 20 min to deprotonate the 2-position followed by quenching with **1**. Deprotection of the hydroxyl group with *p*-toluenesulfonic acid quantitatively generated the terthiophene-substituted **3**. Next, the tripeptide derivative **4** was synthesized according to previously published procedures in 35% yield.[3a] Esterification of compounds **3** and **4** was performed by using *N*-ethyl-*N*′-(dimethylaminopropyl)carbodiimide (EDC) as coupling reagent and 4-(dimethylamino)pyridinium-4-toluenesulfonate (DPTS), a 1:1 complex of *p*-toluenesulfonic acid and 4-(dimethylamino)pyridine, which promotes efficient ester formation at room temperature (Scheme 2).[17] Finally, treatment of **5** with trimethylamine in methanol generated the final product **TTPL**. Because trimethylamine is a relatively weak nucleophile, it was used in large excess (10 equiv) and the reaction mixture was stirred for 7 days at room temperature. **TTPL** was obtained after recrystallization from ethyl acetate. The overall yield of **TTPL** is 8.7%.

2.2. Self-assembly properties and nanostructure morphology observation

The self-assembly properties of **TTPL** were first examined by gelation experiments in various organic solvents. **TTPL** formed a translucent yellow, self-supporting gel at a concentration as low as 1.0 wt % in nonpolar organic solvents such as toluene, benzene, chlorocyclohexane, or chlorobenzene (Table 1). Heating resulted in the transition of the gel state to a clear solution, and gelation was again observed upon cooling. This thermal stimulated gelling process was reversible even after several cycles. Interestingly, gelation did not occur when freshly distilled chlorocyclohexane was used as solvent (1.0 wt %) resulting in precipitation of **TTPL**. The addition of merely 0.1 μl of water regenerated a self-supporting gel after a heating–cooling cycle. Thus, we believe that water molecules are directly involved in the self-assembly process and play an essential role in stabilizing the overall nanostructures. In contrast to the peptide lipids without substitution on the hydrophobic tail, **TTPL**

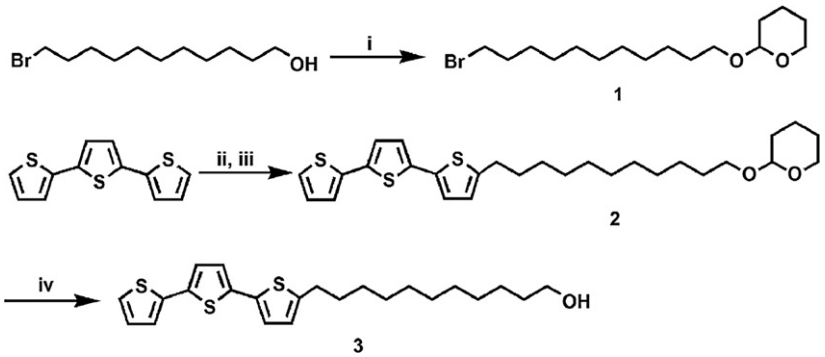

Scheme 1. Synthesis of **3**. Reagents and conditions: (i) *p*-toluenesulfonic acid (TsOH), 3,4-dihydro-2*H*-pyran, CH_2Cl_2, 3 h, 95%; (ii) *n*-butyllithium, THF, −78 °C, 1 h; (iii) **1**, −78 °C→ rt, 18 h, 41%; (iv) TsOH, CH_3OH, 12 h, 100%.

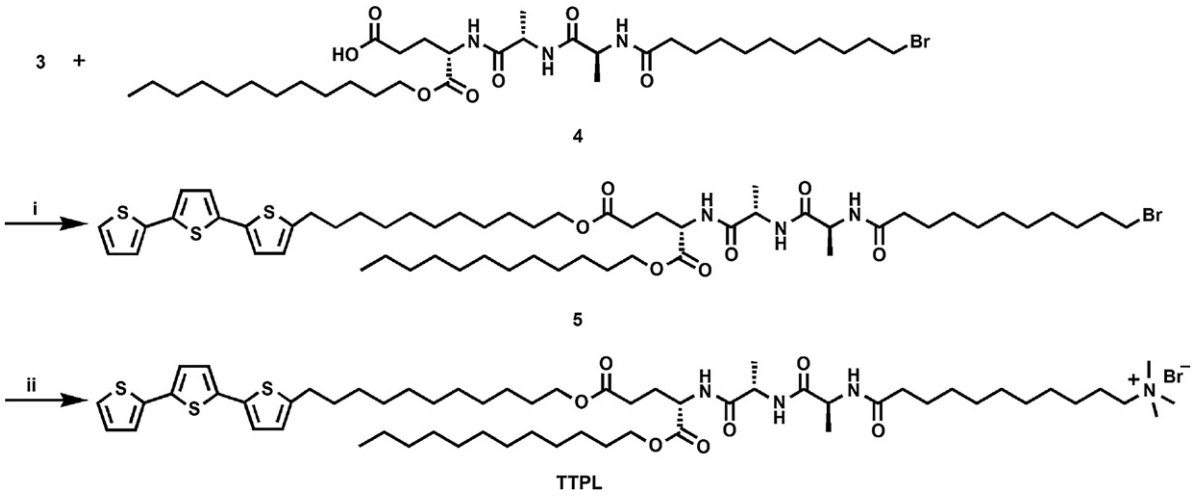

Scheme 2. Synthesis of **TTPL**. Reagents and conditions: (i) *N*-ethyl-*N*′-(dimethylaminopropyl)carbodiimide (EDC), 4-(dimethylamino)pyridinium-4-toluenesulfonate (DPTS), diisopropylethylamine, rt, 18 h, 64%; (ii) NMe_3/methanol, THF, rt, 7 days, 95%.

Table 1
Gelation properties of **TTPL** (1.0 wt %)

Solvent	**TTPL** Solubility[a]
Hexane	I
Cyclohexane	I
Ethyl ether	I
Toluene	G
Benzene	G
Chlorobenzene	G
Chlorocyclohexane	G
Thiophene	G
Dichloromethane	S
Tetrahydrofuran	S
Chloroform	S
Acetone	S
Methanol	S
Acetonitrile	S
DMF	S
Water	I

[a] I: insoluble; G: self-supporting gel; S: solution (condition: 5 mg of **TTPL**, 495 mg solvent, 1.0 wt % in a 2 ml glass vial).

did not cause gelation of water and precipitated presumably due to the substitution of bulkier terthiophene groups.

In many systems, gelation is associated with the formation of one-dimensional nanostructures.[4b] As these high-aspect-ratio nanostructures bundle and entangle into a three-dimensional fibrous network, solvent molecules can be entrapped in the scaffold and result in a decrease in fluidity.[18] Transmission electron microscopy (TEM) was utilized to identify the morphology of the self-assembled nanostructures. To prepare TEM samples, a 1.5 wt % **TTPL** chlorocyclohexane gel was diluted 15-fold to afford a concentration of 0.9 mM followed by drop-casting onto a carbon-coated copper grid. TEM images reveal high-aspect-ratio, cylindrical nanofibers (Fig. 2). The length of these nanofibers varies from 100 nm to over 5 μm. Moreover, TEM images of negatively stained **TTPL** samples clearly show twisted, helical self-assembled nanofibers (Fig. 3). The morphology of a single helix is twisted along the fiber long axis with a diameter of 9±1 nm. In accordance with our proposed model (Fig. 1b), the fiber diameter corresponds to roughly twice the estimated length of a **TTPL** molecule (5.1 nm), suggesting that the width of a single nanofiber is determined by the geometry of two head-to-head **TTPL** molecules. The helical pitch (65±6 nm) of a single helix remains regular along the nanofiber, indicating that the underlying forces causing helix formation are uniform throughout the nanofiber structure. Comparing to our previous

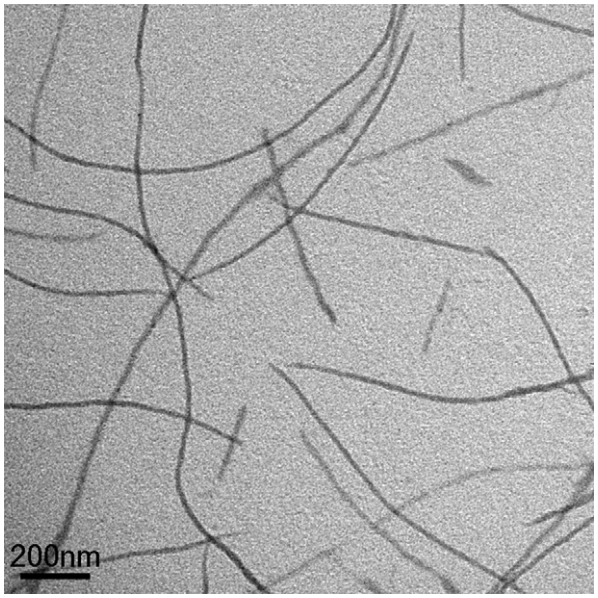

Figure 2. TEM images showing high-aspect-ratio, micrometer-long cylindrical nanofibers of **TTPL**. The sample was drop-cast from a 15-fold diluted solution of 1.5 wt % **TTPL** gel in chlorocyclohexane (0.86 mM). The length of the nanofibers ranges from 100 nm to 5 μm.

results, the substitution of a terthiophene at the periphery did not disrupt nanohelix formation.

Interestingly, TEM images also revealed two other common motifs of double-stranded (Fig. 4) and triple-stranded (Fig. 5) helical nanofibers with diameters of approximately 17 nm and 25 nm, respectively. These double and triple helices appear to be two or three tightly intertwined single helices. Both double and triple helices exhibit a helical pitch of roughly 66 nm, a value very close to the helical pitch of a single helix, indicating that the intertwined single fibers retain their helical structure even after forming larger helices. In addition, parallel bundling of multihelices is also commonly observed on TEM images. Figure 4b and d demonstrate the bundling between double helices. We also observed a single fiber twisted with a double helix to become a bundle (Fig. 5b, see arrows). These results suggest favorable interactions among adjacent single supramolecular fibers to stabilize the overall nanostructure. The helical motifs appear to be basic building blocks connected at

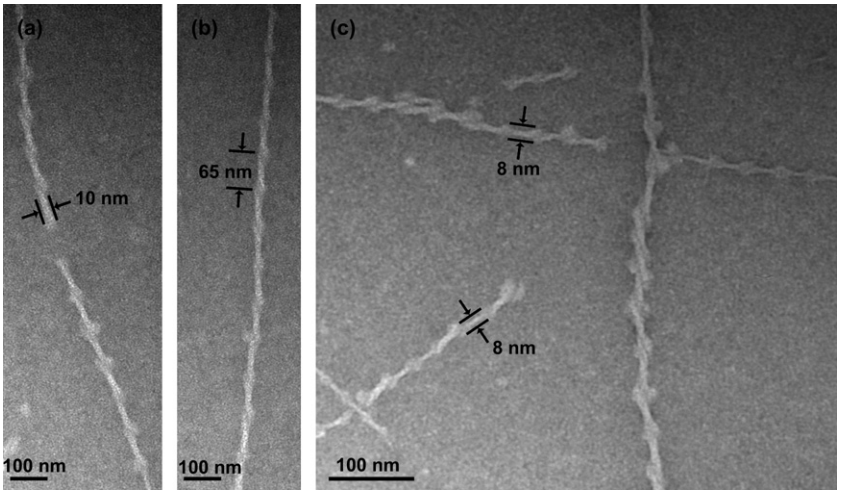

Figure 3. Negatively stained TEM images showing helical **TTPL** nanofibers. The width of a single helix is 9±1 nm. The helical pitch (65±6 nm) remains regular along a single nanofiber. Representative structural parameters are shown in numbers on the graph.

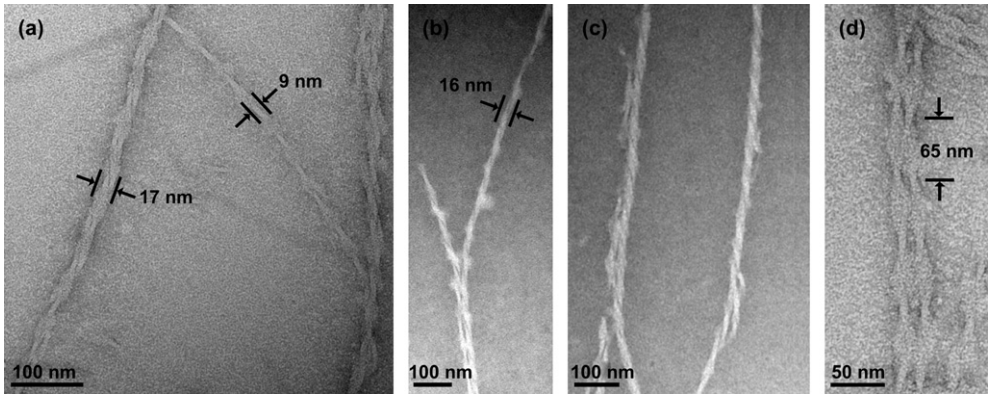

Figure 4. TEM images of **TTPL** nanofibers demonstrating double helical structures. The width of a double helix is 17±1 nm and the helical pitch is 66±5 nm. In panels (b) and (d), we can see parallel bundling of two double helices. Representative structural parameters are shown in numbers on the graph.

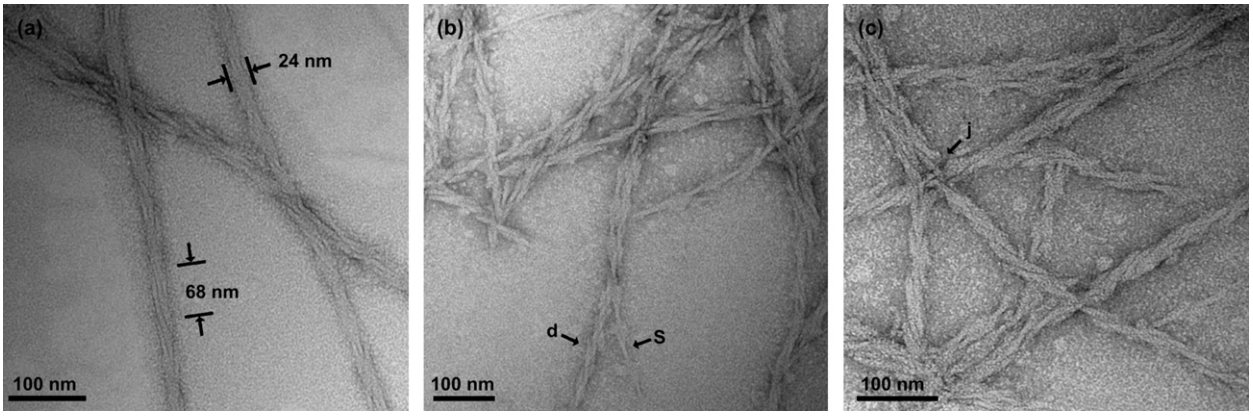

Figure 5. (a) TEM images of the triple helices and bundles of **TTPL** nanofibers. The triple helices have a diameter of 25±2 nm and a helical pitch of 66±8 nm. (b) TEM image of multihelices demonstrating the bundling of a single helix (denoted s) and double helix (denoted d) into a bundle. Higher-order helices are further entangled into a network. (c) TEM image of a helical nanofiber network. A typical junction point (denoted j) of intertwined multihelices is shown.

a junction point to form an entangled network of bundled nanofibers (Fig. 5c). Table 2 summarizes the nanofiber dimensions as determined from TEM images.

This type of hierarchical formation of multihelices is a common supramolecular phenomenon in nature. Collagens, for example, are well known to self-assemble into triple-helical structures consisting of three polypeptide strands that supercoil into a right-handed triple helix.[19] In this case, specific hydrogen bonds between amino acids, especially prolines, hydroprolines, or glycines, and coordination of water molecules serve to stabilize the triple-helical

Table 2
Nanofiber dimensions as determined from TEM images of **TTPL**

	Diameter (nm)	Pitch (nm)
Single helix	9±1	65±6
Double helix	17±1	66±5
Triple helix	25±2	66±8

structure.[20] Synthetic multihelical nanostructures have also been observed in polymeric systems.[21] We recently reported a synthetic peptide amphiphile substituted with a 2-nitrobenzyl group near the β-sheet forming region, and the modification resulted in the formation double or quadruple helical nanofibers compared to the unsubstituted peptide amphiphile, which forms straight cylindrical nanofibers.[22] The tight intertwining of helical nanofibers is presumably due to molecular interactions including hydrogen bonding or hydrophobic effect among neighboring nanofibers. Here, we propose that the formation of higher-order helices is facilitated by the favorable interstrand π–π interaction between terthiophene moieties at the periphery of the nanofibers. In addition, since the helical pitch of a single helix appears to retain after forming multihelices, the structural regularity may also contribute to the formation of stable intertwined structures.

AFM images confirmed that the self-assembled **TTPL** nanofibers adopt a left-handed helical sense (Fig. 6), resembling other unsubstituted PL molecules reported before.[3a] The height of the nanofibers corresponds to the diameter determined by TEM results (9±1 nm). We conclude that **TTPL** self-assembles into chiral helical nanofibers with a regular morphology and uniform left-handed twist. Since these helical nanostructures were imaged by casting a diluted gel on a surface, we cannot rule out the influence of dilution or drying on the observed morphology. Therefore, the structure of the self-assembled nanofibers was further investigated in solution by spectroscopic measurements, which will be discussed in following sections.

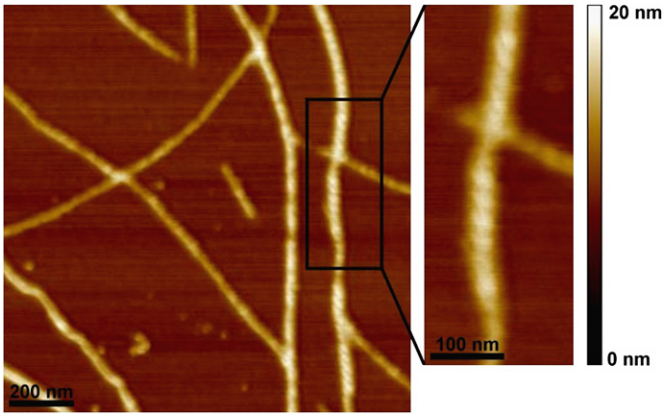

Figure 6. AFM image of **TTPL** nanofibers drop-cast from a diluted **TTPL** chlorocyclohexane solution (0.26 mM) on silicon wafer. The nanofibers exhibit uniformly left-handed helical twist.

2.3. Study of peptide β-sheet structure

FTIR spectroscopy was used to verify the formation of β-sheets within the self-assembled nanostructures of **TTPL**. When peptides form hydrogen-bonded β-sheets, the strength of amide vibrational modes differs due to the elongation of the bond distance. A parallel β-sheet has the characteristic amide A (N–H) absorption at 3271–3285 cm^{-1}, amide I (C=O) at 1635–1639 cm^{-1} and amide II (N–H) at 1540–1549 cm^{-1} while an anti-parallel β-sheet exhibits an additional weak signal around 1690 cm^{-1}.[23] The **TTPL** gel displays IR absorption at 3300 cm^{-1}, 1632 cm^{-1}, and 1541 cm^{-1} corresponding to the signals from parallel β-sheets (see Supplementary data, Fig. S1). The IR result is consistent with our previous findings of other PL molecules, confirming that the substitution of a terthiophene did not disrupt β-sheet formation within the nanostructures.

Circular dichroism (CD) spectra of a **TTPL** gel clearly indicate the presence of peptide β-sheet structures (Fig. 7). At 20 °C, a negative Cotton effect at 220 nm and a positive band at 197 nm are characteristic signals of peptide β-sheets. As the temperature increases, these two signals remain but markedly reduced in intensity. The broadening of the negative Cotton effect at 210 nm implies possible dissociation of β-sheets at higher temperatures.

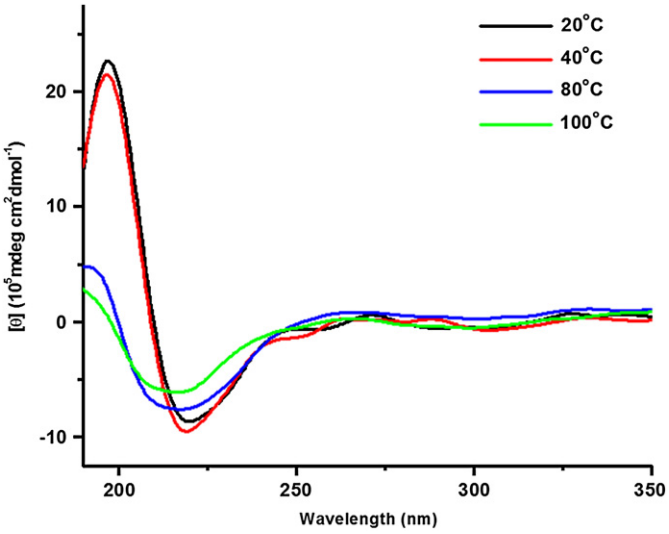

Figure 7. CD spectra of **TTPL** gel (0.75 wt%). The signals at 197 nm and 220 nm indicate the formation of peptide β-sheets. At 80 °C and 100 °C, the negative signal broadens at around 210 nm, implying possible dissociation of β-sheets at higher temperatures.

2.4. Optical properties of TTPL nanostructures

The presence of terthiophene chromophores allows us to obtain structural information from optical properties of **TTPL** in the self-assembled or unassembled state. Figure 8 shows the UV–vis spectra

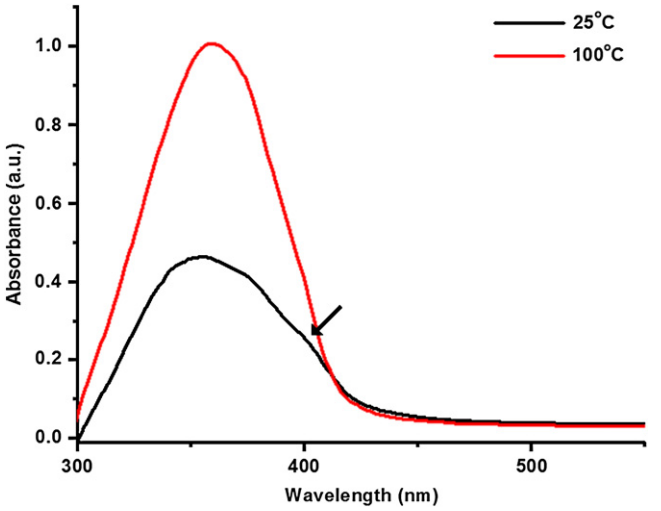

Figure 8. (a) Variable-temperature UV–vis spectra of **TTPL** in chlorocyclohexane (11.5 μM). UV samples were made from dilution of a 1.5 wt% chlorocyclohexane **TTPL** gel. The original absorption maximum intensities were 0.435 at 25 °C (λ_{max}=356 nm, ε=3.78×10^4) and 1.007 at 100 °C (λ_{max}=360 nm, ε=8.75×10^4). The arrow indicates a shoulder around 400 nm at 25 °C.

of **TTPL** in chlorocyclohexane at 25 °C and 100 °C at lower concentration (11.5 μM), respectively. At 25 °C, the UV spectrum exhibits an absorbance peak at 356 nm attributed to the π–π* transition of the terthiophene.[24] After the solution is heated to 100 °C, the absorption λ_{max} remains the same, but the intensity increases 2-fold while the shoulder around 400 nm disappears. Subsequent cooling to 25 °C followed by equilibrating for 1 day restores the intensity and shape of the original spectrum. The decrease in UV–vis absorption at room temperature suggests molecular aggregation of terthiophene moieties, and based on the results from TEM, possibly due to the self-assembly of **TTPL** into nanofibers. Note that the absence of a blue-shifted absorption due to H-aggregates indicates that the terthiophenes are not significantly π–π stacked in either the self-assembled or unassembled state of **TTPL** molecules.[25]

To investigate the chirality of terthiophenes in dilute solution, CD spectra of **TTPL** in chlorocyclohexane and chloroform are compared in Figure 9. At dilute concentration, the **TTPL** solution exhibits Cotton effects with crossover points at 360 nm and 410 nm. The CD spectra of **TTPL** in chloroform were also taken and did not exhibit any CD signal across the spectrum range of 290–550 nm, implying that the conjugated segments are achiral even though the terthiophene is connected via an alkyl linkage to chiral L-amino acids. Thus, the CD signal at 360 nm from terthiophenes in chlorocyclohexane is presumably induced by the formation of chiral helical nanostructures. The positive Cotton effect suggests that the dipole moments of the terthiophenes are oriented in a clockwise direction.[26] In the case of quarter-, quinque-, or sexithiophene derivatives reported by Shinkai et al., the conjugated monomers self-assemble into left-handed helical nanostructures directed by chiral cholesteryl groups.[14] The CD signals of those π–π stacked oligothiophenes exhibit a negative Cotton effect around their UV–vis absorption wavelengths, indicating that the oligothiophenes are aligned in a counterclockwise geometry. The appearance of CD signals demonstrated that the helical nanostructures can transfer chiral information to oligothiophene segments. Since the tripeptide peptide segments self-assemble into β-sheet structures, we assume the molecules are hydrogen-bonded with a right-handed helical twist (resembling β-strands in proteins), so that the dipole moments of terthiophenes afford a clockwise twisting within the nanostructures.

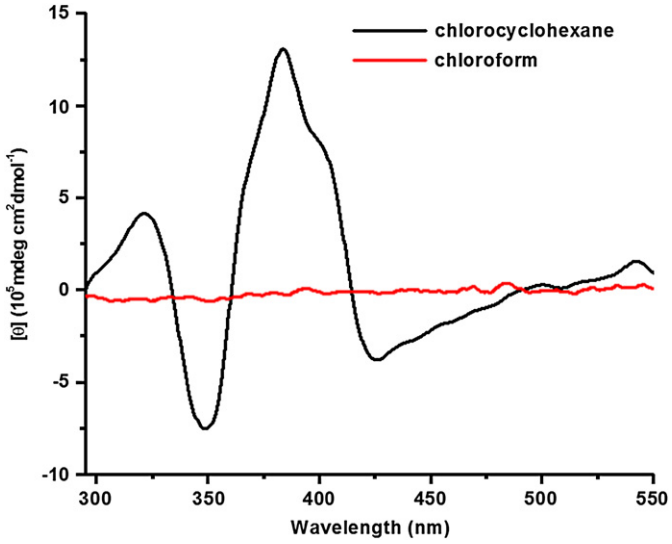

Figure 9. CD spectra of **TTPL** in chlorocyclohexane (black) and in chloroform (red). **TTPL** solution (1.1 mM) exhibits strong Cotton effects at 360 nm and 410 nm, indicating an induced chirality of the terthiophene moieties within the helical nanostructure.

Unexpectedly, the CD spectrum of **TTPL** in chlorocyclohexane shows another Cotton effect signal with crossover point around 410 nm, corresponding to the absorption shoulder in the UV–vis spectrum. This negative Cotton effect suggests the formation of a new optically active species adopting a counterclockwise orientation in the self-assembled state of **TTPL**. We hypothesize that the appearance of the red-shifted band in absorbance spectrum is due to J-aggregation of a fraction of the terthiophene moieties. We mentioned previously the phenomenon of nanofibers intertwining into double or triple-stranded helices. Since the terthiophenes within the nanofibers are aligned perpendicular to the nanofiber long axis, a parallel orientation of interstrand terthiophenes is possible in this geometry. Thus, the exciton coupling of terthiophenes on neighboring nanofibers leads to a 40 nm red-shift of the absorption maximum to 400 nm. Based on AFM images, we know that the helical nanostructures are uniformly left-handed, which presumably directs the orientation of terthiophene J-aggregates and results in the negative Cotton effect in the CD spectrum. Finally, variable-temperature CD spectra show that the signals from aromatic segments disappear at elevated temperatures, indicating a loss of chirality (see Supplementary data, Fig. S2). These spectroscopic observations support our assumption that the terthiophene moieties are in a well-oriented geometry with respect to one another in a concentrated state in chlorocyclohexane due to self-assembly.

The fluorescence emission spectrum of **TTPL** in chlorocyclohexane at 25 °C reveals strong concentration dependence (Fig. 10a). At lower concentrations, the fluorescence shows two bands at 419 nm and 440 nm attributed to the terthiophene emission signals. As the concentration increases, the original emission drastically decreases while two red-shifted emission peaks appear at 471 nm and 502 nm. The corresponding UV–vis spectra at each concentration show no shift of the absorption peak (λ_{max}=356 nm) and follow Beer's law. The quenching of the fluorescence emission is commonly observed in a self-assembled system of chromophores.[4c,14,15] The occurrence of new emission bands in the lower-energy region upon increased concentration suggests that the electronic interactions involved in the aggregation of terthiophene moieties are responsible.[14,27] To support this assumption, a solution of **TTPL** gel was heated to 95 °C to dissociate the self-assembly into monomers (Fig. 10b). An emergence of a new emission peak at 440 nm as well as a 10-fold increase in fluorescence intensity is observed, indicating that the self-assembly of **TTPL** at room temperature is the possible cause for the change in fluorescence emission. Furthermore, we also obtained the UV–vis and fluorescence spectra of **TTPL** in chloroform (see Supplementary data, Figs. S3 and S4). The fluorescence spectra of **TTPL** at different concentrations from 2.9×10^{-3} M to 4.5×10^{-5} M in chloroform shows that the emission maxima remain at 422 nm and 440 nm, whereas the emission intensity increases 500-fold upon dilution by a factor of 64 (see Supplementary data, Fig. S4). The quenching of fluorescence emission at higher concentrations suggests that **TTPL** molecules aggregate in $CHCl_3$ as well.

We conclude from the optical studies that the terthiophene moieties in the self-assembled state in chlorocyclohexane aggregate and display an induced chirality due to the formation of helical nanostructures. Since H-aggregates of terthiophenes of **TTPL** in chlorocyclohexane are not observed, we believe that the β-sheet formation from hydrogen bonding of tripeptides is the dominating force for directing the self-assembly of **TTPL** into one-dimensional nanofibers.

2.5. Variable-temperature NMR (VT-NMR) studies

Variable-temperature ^{1}H NMR of **TTPL** was performed to obtain additional information on molecular interactions in these systems. A solution of **TTPL** in C_6D_6 (3.2 mM) was prepared at room

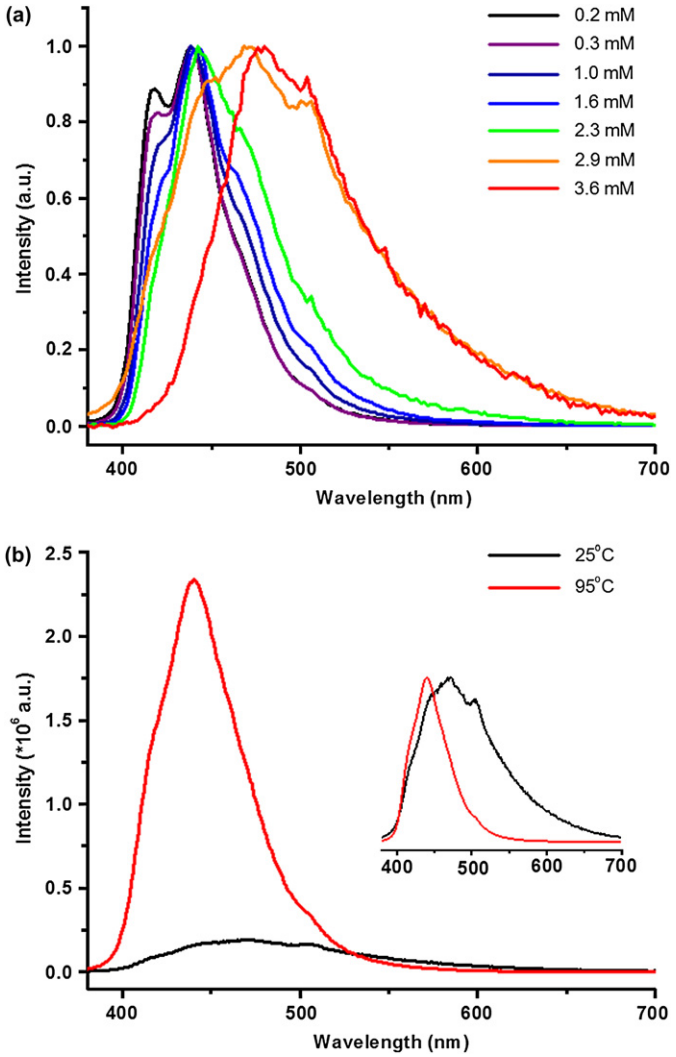

Figure 10. (a) Fluorescence emission of **TTPL** gel of different concentrations at 25 °C. Samples were made from dilution of a 1.5 wt % chlorocyclohexane **TTPL** gel (12.9 mM) from 25 μl (black), 50 μl (purple), 150 μl (navy), 250 μl (blue), 350 μl (green), 450 μl (orange), or 550 μl (red) to 2 ml. The excitation wavelength is 360 nm. Graphs are normalized to show relative peak positions. (b) Fluorescence spectra of **TTPL** in chlorocyclohexane at 25 °C and 95 °C (excited at 360 nm). A 10-fold quenching of emission intensity is observed at 25 °C, indicating strong aggregation of terthiophene moieties. The intensity of emission maxima is 2.34×10^5 at 95 °C (λ_{max}=440 nm, red line) and 1.92×10^4 at 25 °C (λ_{max}=471 nm, black line). The inset graph shows normalized peaks for comparison.

temperature. Gelation was induced and the NMR spectrum showed complete line broadening. This viscous gel was heated up to 70 °C initially followed by cooling down, and measurements were taken every 5 °C from 70 °C to 25 °C. Selected spectra are shown in Figure 11. The NMR spectra at temperature 70–50 °C are relatively resolved, indicating that **TTPL** molecules are unassembled. Also, three doublets assigned to amide protons were shifted downfield

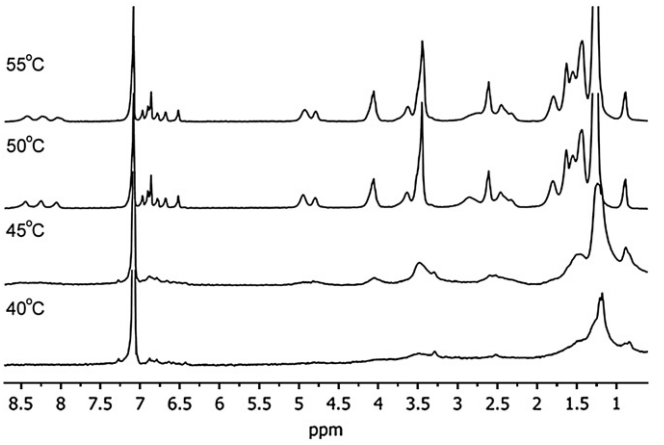

Figure 11. Variable-temperature ^{1}H NMR spectra of a **TTPL** in C_6D_6 (3.2 mM) at 55 °C, 50 °C, 45 °C, and 40 °C.

by 0.1–0.2 ppm upon cooling to 50 °C. The de-shielding effect is attributed to intermolecular hydrogen bonding that decreases the electron density around the N–H protons. Spectra below 50 °C display a significant line broadening of all protons because of the self-assembly of **TTPL** molecules, indicating that the transition temperature (T_{gel}) of **TTPL** monomers to the self-assembled state is around 45–50 °C.

Similarly, a VT-NMR experiment was done with **TTPL** in $CDCl_3$ (3.2 mM). The sample was heated to 55 °C initially and gradually cooled to 22 °C (see Supplementary data, Fig. S5). Again, a downfield shift about 0.2 ppm of three amide protons is observed upon cooling, indicating possible hydrogen bonding of the amide groups. This finding is in accordance with our fluorescence studies of **TTPL** in $CHCl_3$ that aggregation of terthiophenes is observed even at a concentration range of 10^{-3}–10^{-5} M (see Supplementary data, Fig. S4). Other NMR peaks assigned to terthiophenes or alkyl chains remain the same over the temperature range, indicating a lack of interaction of these functional groups in $CDCl_3$.

2.6. Peptide stereochemistry and self-assembly

We have described above the influence of π–π interactions from terthiophene groups on the self-assembly of helical nanofibers. Next, we investigated how peptide stereochemistry impacts the nature of the self-assembled nanostructures. Peptide lipid **6a** was previously synthesized containing a *p*-toluene carboxylate ester as the endgroup on the PL backbone.[3a] We reported that peptide lipid **6a** caused gelation of nonpolar organic solvents, and the AFM images revealed uniformly left-handed helical nanofiber formation with a pitch of 160±30 nm. Three diastereomers **6b**–**6d** were synthesized following the same procedures for **6a** but using both L- and D-alanine to reveal the role of stereochemistry of the dialanine on nanofiber morphology (Fig. 12).

Compounds **6b** and **6c** form organogels in nonpolar organic solvents resembling the behavior of **6a**. Despite the structural

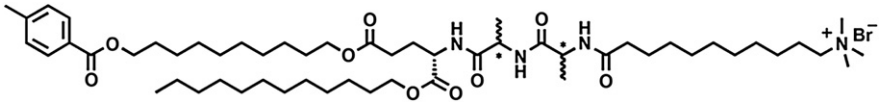

6a (LLL): L-Glu, L-Ala, L-Ala
6b (LLD): L-Glu, L-Ala, D-Ala
6c (LDD): L-Glu, D-Ala, D-Ala
6d (LDL): L-Glu, D-Ala, L-Ala

Figure 12. Chemical structure of molecules **6a**–**6d**.

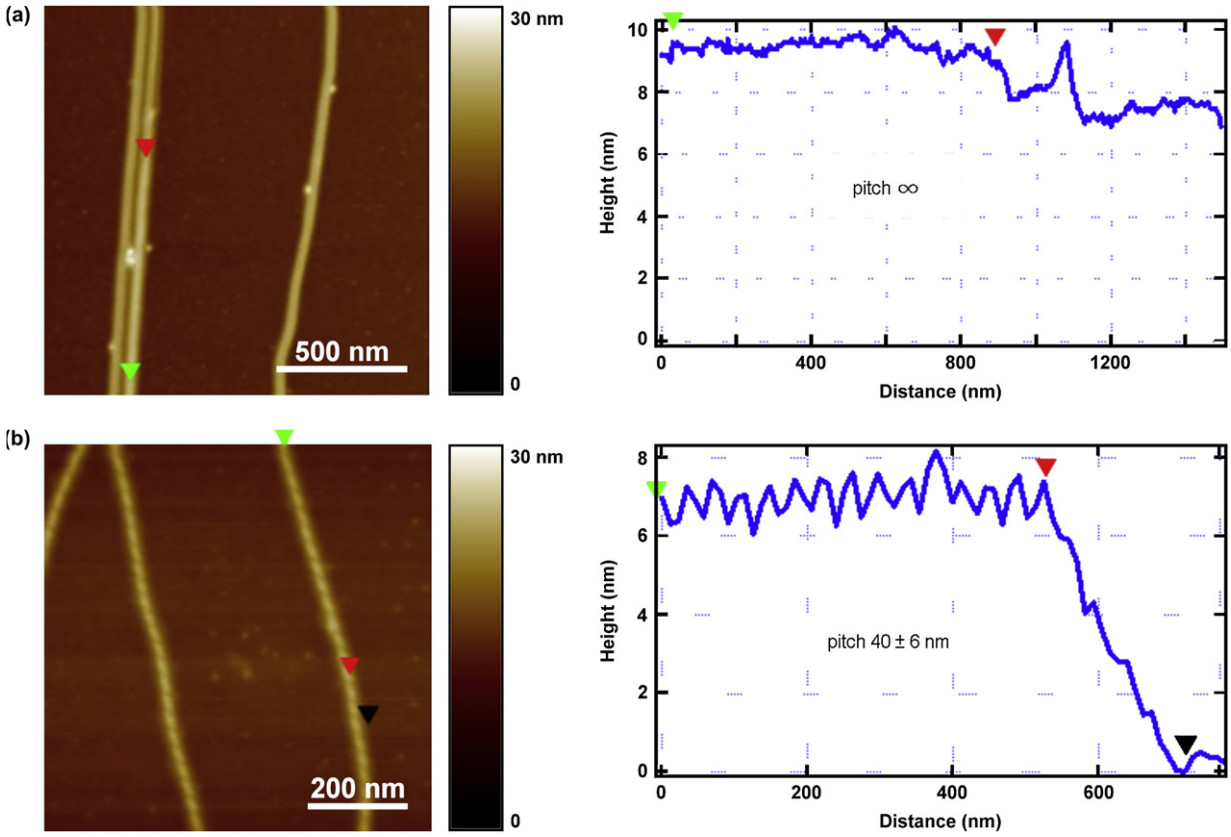

Figure 13. AFM images (left) and corresponding height profiles (right) of molecules (a) **6b** (**LLD**) and (b) **6c** (**LDD**). Molecule **6b** forms a straight cylindrical nanofiber while **6c** forms helical nanofibers with a pitch of 40±6 nm.

similarity, molecule **6d** does not form a gel in nonpolar solvents and precipitates from solution, indicating that one-dimensional self-assembly does not occur in this case. AFM images confirm that molecules **6b** and **6c** self-assemble into micrometer-long nanofibers in chlorocyclohexane with a diameter of 9±1 nm (Fig. 13). Remarkably, for **LLD** (**6b**) in which the second alanine farthest from the L-glutamic acid is changed to D-alanine, cylindrical nanofibers are formed with no twisting (Fig. 13a). When the other alanine is also changed to D-alanine (**LDD**, **6c**), we again observed left-handed helical nanofibers with a regular periodicity of 40±6 nm, significantly smaller than the pitch of **LLL** nanofibers (Fig. 13b). AFM samples of molecule **6d** in chlorocyclohexane only contain irregular aggregates. We conclude that the stereochemistry strongly influences the mechanism for helical nanofiber formation. In a polypeptide system of $(Leu)_4(Lys)_8(Leu)_4$ reported by Higashi et al., the helical sense of one-dimensional nanofibers can be inverted from left-handed to right-handed by changing the stereochemistry of amino acids from L- to D-isomer, suggesting that the intrinsic chirality of a β-sheet directly affects nanohelix formation.[28] Moreover, it was shown by Rowan et al. that the conformation and stability of a helical poly(isocyanopeptides) are influenced by the stereochemistry of the di- or trialanine segments on the polymer backbone.[29] They proposed that the different steric hindrance of substituents on the amino acids results in different strengths for hydrogen bonds. In our system, we hypothesize that the steric effects of amino acids in hydrogen-bonded structures may affect the properties (conformation or strength) of the primary β-helix, which directly influences the secondary superhelix formation. For compound **LDL** (**6d**), the alternating substituents on the chiral centers may cause a steric hindrance that disrupts proper stacking of tripeptides, and as a result, the formation of β-sheets is inhibited.

3. Conclusion

Molecules combining a conjugated segment of potential interest in electronic properties with peptide segments were found to self-assemble into high-aspect-ratio, left-handed helical nanofibers with regular diameter and pitch. Peptide segments were found to dominate self-assembly by forming β-sheet structures that induce chirality in conjugated terthiophene segments. The conjugated structures appear to form J-aggregates between fibers as evidenced by the formation of double- and triple-stranded nanostructures as well as spectroscopic measurements. Secondly, our study on the effect of peptide stereochemistry on self-assembly confirms the essential role of the primary β-helix on self-assembly of these systems into one-dimensional nanostructures. Stereochemical changes in diastereomeric sequences of the tripeptide segment were found to be sufficient to suppress one-dimensional self-assembly or supercoiling of the supramolecular aggregates. We believe these effects are steric in nature and could be used to design novel strategies to optimize the morphology and properties of nanostructures based on these amphiphilic molecules.

4. Experimental

4.1. General

All chemicals were purchased from commercial sources (Sigma–Aldrich, Alfa Aesar, TCI, or Advanced ChemTech) and used without further purification unless otherwise noted. Deuterated solvents were purchased from Cambridge Isotope Laboratories, Inc. Chlorocyclohexane was distilled and saturated with water before usage.

All NMR spectra were taken with compound concentrations of 1–5 mM in $CDCl_3$ or C_6D_6. ^1H NMR and ^{13}C NMR were recorded on

Varian 400 MHz or 500 MHz NMR Spectrometer at 295 K. The molecular weight of compounds was analyzed by using a PE Voyager DE-Pro MALDI-TOF-MS instrument. High-resolution mass spectra were recorded on an Agilent 6210 LC-TOF spectrometer with Agilent 1200 HPLC introduction. FTIR data was obtained using a Fourier transform IR spectrometer (Thermo Nicolet, Nexus 870 with the Tabletop optics module). Optical rotation value $[\alpha]_D$ was decided by placing a solution (0.7 ml) in a stainless steel tube with path length of 100 mm, followed by measurement using a type AA-100 automatic polarimeter (Optical Activity Ltd.).

For optical measurements, circular dichroism (CD) spectra were recorded on a JascoModel J-715 Circular Dichroism Spectrometer operating between 250 nm and 700 nm using a quartz cell with path length of 1 mm. UV–vis spectra were collected on a Varian Cary 500 UV/VIS/NIR Spectrometer using a quartz cell (Fisher Scientific, Inc.) of 1 cm path length. Fluorescence spectra were performed on an ISS PC1 Photon Counting Fluorometer using the same quartz cells. All emission spectra were collected at 90° angle at room temperature.

The molecular lengths of PLs were estimated by molecular mechanics calculation performed with MM2 force field as implemented in the software Chem3D Pro 8.0 (CambridgeSoft Corporation).

4.2. Gelation

For a typical gelation experiment, 5–10 mg of the peptide lipid was mixed with gelation solvent, such as chlorocyclohexane or toluene, to give a concentration of 1.5 wt %. The solution was kept in a tightly capped vial, heated up to the boiling point of the solution, and cooled down to room temperature. A self-supporting gel formed within 30 min.

4.3. Transmission electron microscope (TEM)

To prepare a TEM sample, the self-assembled chlorocyclohexane gel (1.5 wt %) was diluted 15-fold (20 μl gel into 280 μl solvent, 0.86 mM) and vortex mixed for about 30 s. A small volume (~5 μl) of this solution was deposited onto a carbon-coated copper grid. Excess solution was quickly wicked away by a piece of filter paper and the samples were subsequently dried in air. Once dried, the samples were negatively stained by placing a drop of 2 wt % uranyl acetate aqueous solution on the grid. A thin layer of uranyl acetate was left on the grid after blotting away excess staining solution. The samples were again dried in ambient conditions. Bright-field TEM imaging of the assembled nanostructures was performed on a JEOL 1230 Transmission Electron Microscope, operating at 100 kV.

4.4. Atomic force microscopy (AFM)

For sample preparation, silicon wafers with a (111) surface were used as substrates (Silicon Quest International, Inc.). The surface was cleaned with ultrasonication in deionized water, acetone, and 2-propanol for 15 min each, and subsequently dried under nitrogen flow. An aliquot of 10 μl of the 1.5 wt % chlorocyclohexane gel was diluted 50-fold with the same solvent (0.26 mM). After vortex mixing for 1 min, 0.1 μl of the diluted solution was drop-cast on the silicon surface and the solvent was evaporated in air. AFM experiments were performed immediately following sample preparation.

All AFM images were recorded under ambient conditions on a Multimode scanning probe microscope from Digital Instruments. Tapping-mode AFM technique was chosen to measure the morphology of the self-assembled PLs in order to minimize shear forces, which can cause distortion of the nanostructures and inaccuracy of the topology. Silicon cantilevers purchased from Asylum Research (AC240TS) were used in all AFM experiments.

4.5. Variable-temperature ^{1}H NMR spectra

Variable-temperature ^{1}H NMR spectra were performed on a Varian 400 MHz NMR Spectrometer. Samples were prepared by dissolving 3.0 mg **TTPL** in 0.8 ml in $CDCl_3$ or C_6D_6 in an NMR tube (3.2 mM). For C_6D_6, the solution was warmed up to a homogeneous state using a heat gun. Gelation of C_6D_6 occurred immediately upon cooling back to room temperature. The NMR samples were heated up to the highest set temperature and gradually cooled down. Each measurement was taken after equilibrating at a temperature for 10 min.

4.6. Variable-temperature optical measurements

Samples of **TTPL** in chlorocyclohexane were prepared from dilution of a 1.5 wt % gel. Measurements were taken immediately following sample preparation at 25 °C. Samples were heated to the desired temperature and equilibrated for 15 min before measurement.

4.7. Synthesis

Synthesis of 4-(dimethylamino)pyridinium-4-toluenesulfonate (DPTS)[16] and compounds **1**,[3a] **4**,[3a] and **6a**[3a] were reported previously. Compounds were purified by preparative column chromatography using silica gel (Bodman Industries, 32–63 μm, 60 Å). Reaction intermediates were monitored by analytical thin-layer chromatography (TLC) performed on Merck KGaA silica gel 60 F_{254} TLC plates.

*4.7.1. Compound **2***

To an oven-dried flask containing terthiophene (0.72 g, 2.90 mmol) and a stir bar was added anhydrous THF (10 ml) and capped. The solution was rigorously degassed with N_2 flow for 20 min before cooled to −78 °C, and *n*-butyllithium (1.16 ml of 2.5 M solution, 2.90 mmol) was introduced dropwise by a syringe in 10 min. The solution was stirred for another 10 min before adding compound **1** (0.97 g, 2.90 mmol), and the mixture was slowly warmed up to room temperature. After 20 h, water was added to the flask to quench the reaction, and the resultant mixture was stirred for 30 min before removing THF under reduced pressure at 40 °C. The residue was redissolved in dichloromethane and extracted with saturated $NaHCO_{3(aq)}\times 1$, water×1, and brine×1. The organic layer was dried over anhydrous $MgSO_4$ and evaporated to dryness under reduced pressure. The concentrated residue was purified by column chromatography on silica gel with gradient CH_2Cl_2/hexane (1:8, 1:6, 1:5, and 1:3) as eluent to allow isolation of **2** in 41% yield as a brown liquid (0.60 g, 1.19 mmol). ^{1}H NMR (500 MHz, $CDCl_3$): δ 7.22(d, J=4.5 Hz, 1H), 7.17 (d, J=3.5 Hz, 1H), 7.07 (d, J=3.5 Hz, 1H), 7.02 (dd, J=4.5, 3.5 Hz, 1H), 7.01 (d, J=3.5 Hz, 1H), 6.99 (d, J=3.5 Hz, 1H), 6.69 (d, J=3.5 Hz, 1H), 4.58 (d, 3.5 Hz, 1H, O–C*H*–O), 3.88 (m, 1H, $-C_{(ring)}HH'-O-$), 3.74 (m, 1H, $-C_{(ring)}HH'-O-$), 3.51 (m, 1H, –C*H*H′–O–), 3.39 (m, 1H, –CH*H*′–O–), 2.80 (t, J=7.5 Hz, 2H), 1.85 (m, 1H), 1.71 (m, 3H), 1.67–1.48 (m, 4H), 1.47–1.25 (m, 16H). ^{13}C NMR (125 MHz, $CDCl_3$): δ 145.79, 137.48, 137.00, 135.66, 134.63, 128.02, 125.01, 124.44, 124.43, 123.67, 123.54, 99.05, 67.89, 62.55, 33.03, 31.79, 30.98, 30.38, 29.77, 29.71, 29.61, 29.54, 29.27, 28.96, 26.44, 25.70, 19.91. HRMS-ESI (m/z): $[M+H]^+$ calcd for $C_{28}H_{39}O_2S_3$ 502.2034; found 502.2028.

*4.7.2. Compound **3***

To a solution of compound **2** (0.44 g, 0.88 mmol) in methanol (10 ml) and CH_2Cl_2 (10 ml) was added *p*-toluenesulfonic acid

monohydrate (12 mg, 0.063 mmol) and the reaction mixture was stirred for 12 h at room temperature. The solvent was removed under reduced pressure, and the residue was redissolved in CH_2Cl_2 followed by extraction with saturated $NaHCO_{3(aq)}\times 2$ and water×1. The organic layer was dried over anhydrous $MgSO_4$ and evaporated to dryness under reduced pressure. Column chromatography of the resultant solid on silica gel with CH_2Cl_2/hexane (2:1) as eluent afforded compound **3** quantitatively as a yellow solid (0.36 g, 0.88 mmol). ^{1}H NMR (500 MHz, $CDCl_3$): δ 7.22(d, J=4.5 Hz, 1H), 7.17 (d, J=3.5 Hz, 1H), 7.07 (d, J=3.5 Hz, 1H), 7.03 (dd, J=4.5, 3.5 Hz, 1H), 7.01 (d, J=3.5 Hz, 1H), 6.99 (d, J=3.5 Hz, 1H), 6.70 (d, J=3.5 Hz, 1H), 3.66 (t, J=6.5 Hz, 2H, –CH_2–OC(O)–), 2.81 (t, J=7.5 Hz, 2H), 1.70 (m, 2H), 1.58 (m, 2H), 1.49–1.25 (m, 14H). ^{13}C NMR (125 MHz, $CDCl_3$): δ 145.81, 137.49, 137.02, 135.68, 134.66, 128.05, 125.03, 124.48, 124.46, 123.69, 123.56, 63.31, 33.01, 31.80, 30.39, 29.79, 29.75, 29.63, 29.55, 29.27, 29.00, 25.95. HRMS-ESI (m/z): $[M+H]^+$ calcd for $C_{23}H_{31}OS_3$ 418.1459; found 418.1458.

4.7.3. Compound **5**

To a solution of compound **3** (0.30 g, 0.72 mmol) and compound **4** (0.50 g, 0.71 mmol) in CH_2Cl_2 (50 ml) were added EDC (0.15 g, 0.78 mmol), DPTS (0.24 g, 0.82 mmol), and diisopropylethylamine (0.2 ml). The reaction mixture was stirred at room temperature for 20 h. The solution was extracted with $NaHCO_{3(aq)}\times 1$, brine×1, and water×2 to remove EDC and DPTS, and then the organic layer was dried over anhydrous $MgSO_4$ before evaporation to dryness under reduced pressure. The crude product was purified by column on silica gel using CH_2Cl_2 and CH_2Cl_2/CH_3OH (99:1, 98:2, and 95:5) as eluents to isolate compound **5** as a yellow solid in 64% yield (0.50 g, 0.45 mmol). ^{1}H NMR (500 MHz, $CDCl_3$): δ 7.72 (d, J=7.5 Hz, 1H, NH), 7.55 (d, J=7.0 Hz, 1H, NH), 7.19 (d, J=5.0 Hz, 1H), 7.14 (d, J=3.5 Hz, 1H), 7.05–6.96 (m, 5H), 6.67 (d, J=3.0 Hz, 1H), 4.77 (m, 2H), 4.60 (q, J=6.0 Hz, 1H), 4.12 (m, 3H), 4.04 (t, J=6.5 Hz, 3H), 3.38 (t, J=7.0 Hz, 3H, CH_2Br), 2.78 (t, J=7.5 Hz, 2H, –$C_{(ring)}CH_2$), 2.39 (m, 2H), 2.25 (t, J=8.0 Hz, 2H), 2.20 (m, 1H), 2.02 (m, 1H), 1.84 (m, 2H), 1.70–1.58 (m, 8H), 1.40 (d, J=6.5 Hz, 3H), 1.37 (d, J=7.0 Hz, 3H), 1.37–1.22 (m, 38H), 0.88 (t, J=6.0 Hz, 3H). ^{13}C NMR (125 MHz, $CDCl_3$): δ 173.19, 172.81, 172.63, 172.38, 171.80, 145.61, 137.38, 136.90, 135.59, 134.58, 127.95, 124.93, 124.36, 124.33, 123.57, 123.43, 65.86, 65.03, 51.80, 48.97, 48.69, 36.43, 34.06, 32.94, 32.05, 31.72, 30.41, 30.30, 29.80, 29.78, 29.75, 29.71, 29.67, 29.58, 29.54, 29.50, 29.42, 29.40, 29.21, 28.91, 28.72, 28.65, 28.30, 27.50, 26.02, 25.97, 25.82, 22.82, 22.79, 19.55, 19.28, 14.26. IR (NaCl): ν=3288 (br, NH stretch), 3069 (=C–H stretch), 2927 (CH antisym and sym stretch), 2847 (CH antisym and sym stretch), 1739 (C=O stretch), 1629 (C=O stretch, amide I band), 1562, 1537 (NH deformation, amide II band), 1454, 1394, 1268, 1204, 1169, 1062, 987, 793, 713 cm^{-1}. $[\alpha]_D^{20}$ −0.28 (c 2.00, $CHCl_3$). MS-ESI (m/z): $[M+H]^+$ calcd for $C_{57}H_{90}BrN_3O_7S_3$ 1103.5; found 1104.5. HRMS-ESI (m/z): $[M+H]^+$ calcd for $C_{57}H_{90}BrN_3O_7S_3$ 1103.5124; found 1103.5115.

4.7.4. Compound **TTPL**

To a solution of compound **5** (0.40 g, 0.36 mmol) in THF (10 ml) was added trimethylamine (3 ml of 4.2 M solution, 12.6 mmol) and allowed to stir for 7 days at room temperature. The reaction solution was evaporated to give a yellow solid. Subsequently recrystallization from ethyl acetate afforded **TTPL** in 95% yield (0.38 g, 0.34 mmol) as a yellow solid. ^{1}H NMR (500 MHz, $CDCl_3$): δ 7.48 (d, J=8.5 Hz, 1H, NH), 7.29 (d, J=9.0 Hz, 1H, NH), 7.17 (d, J=6.5 Hz, 1H), 7.12 (d, J=8.5 Hz, 1H), 7.02 (d, J=4.0 Hz, 1H), 6.99–6.93 (m, 3H), 6.90 (d, J=8.5 Hz, 1H, NH), 6.65 (d, J=3.5 Hz, 1H), 4.50 (m, 3H), 4.10 (t, J=8.5 Hz, 2H), 4.05 (t, J=8.0 Hz, 2H), 3.58 (br, 2H, –CH_2NMe_3), 3.42 (s, 9H, NCH_3), 2.80 (t, J=9.5 Hz, 2H, –$C_{(ring)}CH_2$), 2.41 (m, 2H), 2.31 (t, J=8.0 Hz, 2H), 2.20 (m, 1H), 2.05 (m, 1H), 1.80 (m, 2H), 1.63 (m, 8H), 1.44 (d, J=8.5 Hz, 3H), 1.40–1.26 (m, 41H), 0.89 (t, J=6.8 Hz, 3H). ^{13}C NMR (125 MHz, $CDCl_3$): δ 173.14, 172.84, 172.52, 172.41, 171.85, 145.82, 137.39, 137.00, 135.67, 134.62, 128.07, 125.05, 124.50, 124.46, 123.70, 123.57, 65.90, 65.12, 53.70, 52.08, 49.53, 32.13, 31.81, 30.58, 30.39, 29.85, 29.82, 29.73, 29.57, 29.47, 29.46, 29.29, 28.91, 28.71, 28.60, 28.58, 28.45, 27.24, 26.11, 26.04, 22.90, 18.60, 18.36, 14.38. IR (NaCl): ν=3293 (br, NH stretch), 3070 (=C–H stretch), 2922 (CH antisym and sym stretch), 2851 (CH antisym and sym stretch), 1732 (C=O stretch), 1632 (C=O stretch, amide I band), 1534 (NH deformation, amide II band), 1465, 1450, 1395, 1368, 1203, 1169, 1056, 963, 915, 838, 790, 753, 694 cm^{-1}. $[\alpha]_D^{20}$ −0.73 (c 1.50, $CHCl_3$). HRMS-ESI (m/z): $[M-Br]^+$ calcd for $C_{60}H_{99}N_4O_7S_3$ 1083.6676; found 1083.6686.

4.7.5. Compounds **6b**, **6c**, and **6d**

The synthesis of compound **6b**–**6d** followed the same published procedures as compound **6a** using corresponding L- and D-amino acids.[3a]

*4.7.5.1. Compound **6b** (**LLD**).* ^{1}H NMR (500 MHz, $CDCl_3$): δ 7.90(d, J=8.0 Hz, 2H), 7.48 (br, 2H), 7.21 (d, J=8.0 Hz, 2H), 4.50 (m, 3H), 4.26 (br, 2H), 4.01 (t, J=7.0 Hz, 2H), 3.57 (m, 2H), 3.39 (s, 9H), 2.40 (m, 5H), 2.25 (t, J=7.5 Hz, 2H), 2.20 (m, 1H), 2.05 (m, 1H), 1.76 (m, 2H), 1.62 (m, 8H), 1.50–1.18 (m, 48H), 0.89 (t, J=6.5 Hz, 3H). ^{13}C NMR (125 MHz, $CDCl_3$): δ 173.96, 173.26, 173.16, 172.79, 171.86, 167.04, 143.71, 129.76, 129.28, 127.92, 67.07, 65.82, 65.16, 65.12, 53.64, 52.09, 49.55, 36.26, 32.14, 30.68, 29.87, 29.76, 29.69, 29.58, 29.49, 28.94, 28.79, 28.73, 27.11, 26.25, 26.13, 26.06, 25.50, 23.12, 22.92, 21.90, 18.28, 18.13, 14.40. IR (NaCl): ν=3272 (br, NH stretch), 3043 (=C–H stretch), 2953 (CH antisym and sym stretch), 2854 (CH antisym and sym stretch), 1735 (C=O stretch), 1660 (C=O stretch, amide I band), 1534 (NH deformation, amide II band), 1453, 1371, 1274, 1177, 1107, 1017, 962, 906, 836, 755 cm^{-1}. $[\alpha]_D^{20}$ +0.25 (c 2.00, $CHCl_3$). HRMS-ESI (m/z): $[M-Br]^+$ calcd for $C_{55}H_{97}N_4O_9$ 957.7256; found 957.7242.

*4.7.5.2. Compound **6c** (**LDD**).* ^{1}H NMR (500 MHz, $CDCl_3$): δ 7.90 (d, J=8.0 Hz, 2H), 7.47 (d, 1H), 7.39 (d, 1H), 7.21 (d, J=8.0 Hz, 2H), 4.50 (m, 3H), 4.26 (br, 2H), 4.01 (t, J=7.0 Hz, 2H), 3.57 (m, 2H), 3.39 (s, 9H), 2.40 (m, 5H), 2.25 (t, J=7.5 Hz, 2H), 2.20 (m, 1H), 2.05 (m, 1H), 1.76 (m, 2H), 1.62 (m, 8H), 1.50–1.18 (m, 48H), 0.89 (t, J=6.5 Hz, 3H). ^{13}C NMR (125 MHz, $CDCl_3$): δ 174.36, 173.29, 173.17, 172.84, 172.06, 167.05, 143.71, 129.76, 129.28, 127.93, 67.07, 65.89, 65.17, 65.09, 53.66, 52.03, 49.44, 36.23, 32.13, 30.59, 29.86, 29.75, 29.69, 29.58, 29.49, 28.95, 28.82, 28.73, 27.09, 26.25, 26.06, 26.05, 25.48, 23.13, 22.92, 21.90, 18.18, 18.05, 14.37. IR (NaCl): ν=3288 (br, NH stretch), 3058 (=C–H stretch), 2922 (CH antisym and sym stretch), 2852 (CH antisym and sym stretch), 1731 (C=O stretch), 1632 (C=O stretch, amide I band), 1544 (NH deformation, amide II band), 1465, 1450, 1397, 1365, 1327, 1276, 1200, 1160, 1066, 967, 910, 722, 694 cm^{-1}. $[\alpha]_D^{20}$ +0.55 (c 2.00, $CHCl_3$). HRMS-ESI (m/z): $[M-Br]^+$ calcd for $C_{55}H_{97}N_4O_9$ 957.7256; found 957.7240.

*4.7.5.3. Compound **6d** (**LDL**).* ^{1}H NMR (500 MHz, $CDCl_3$): δ 7.90 (d, J=8.0 Hz, 2H), 7.59 (d, 1H), 7.46 (d, 1H), 7.22 (d, J=8.0 Hz, 2H), 7.13 (d, 1H), 4.50–4.26 (m, 5H), 4.01 (t, J=7.0 Hz, 2H), 3.57 (m, 2H), 3.39 (s, 9H), 2.39 (m, 5H), 2.24 (t, J=7.5 Hz, 2H), 2.20 (m, 1H), 2.05 (m, 1H), 1.75 (m, 2H), 1.59 (m, 8H), 1.50–1.18 (m, 48H), 0.86 (t, J=6.5 Hz, 3H). ^{13}C NMR (125 MHz, $CDCl_3$): δ 173.96, 173.31, 173.14, 172.97, 172.21, 167.04, 143.70, 129.76, 129.28, 127.95, 67.06, 65.83, 65.16, 65.05, 53.64, 52.04, 49.62, 36.20, 32.13, 30.69, 29.86, 29.75, 29.68, 29.57, 29.49, 28.95, 28.79, 28.73, 27.09, 26.25, 26.11, 25.48, 23.10, 22.91, 21.89, 18.12, 18.03, 14.36. IR (NaCl): ν=3250 (br, NH stretch), 3030 (=C–H stretch), 2926 (CH antisym and sym stretch), 2854 (CH antisym and sym stretch), 1736 (C=O stretch), 1658 (C=O stretch, amide I band), 1536 (NH deformation, amide II band), 1454, 1380, 1274, 1211, 1177, 1107, 1020, 970, 902, 838, 755, 721, 690 cm^{-1}. $[\alpha]_D^{20}$

−0.07 (*c* 2.00, $CHCl_3$). HRMS-ESI (*m*/*z*): $[M-Br]^+$ calcd for $C_{55}H_{97}N_4O_9$ (M^+) 957.7256; found 957.7240.

Acknowledgements

This research was supported by grants from the National Science Foundation (DMR-0605427), the U.S. Department of Energy (DE-FG02-00ER45810), and the National Science Foundation—Nanoscale Science and Engineering Center at Northwestern University (NSEC EEC-0118025). The authors are grateful for the use of the following shared facilities at Northwestern University: IMSERC, BIF, Keck Biophysics, and NUANCE Center (EPIC, NIFTI, Keck-II facility). We also thank Liam Palmer of the authors' laboratory for valuable discussions.

Supplementary data

Supplementary data includes FTIR spectrum of **TTPL** chlorocyclohexane gel (Fig. S1), variable-temperature CD spectra of **TTPL** solution (Fig. S2), UV–vis and fluorescence spectra of **TTPL** in chloroform (Fig. S3), concentration study of **TTPL** fluorescence emission in chloroform (Fig. S4), and variable-temperature NMR study of **TTPL** in $CDCl_3$ (Fig. S5). Supplementary data associated with this article can be found in the online version, at doi:10.1016/j.tet.2008.06.033.

References and notes

1. (a) Cornelissen, J. J. L. M.; Rowan, A. E.; Nolte, R. J. M.; Sommerdijk, N. A. J. M. *Chem. Rev.* **2001**, *101*, 4039–4070; (b) Palmer, L. C.; Velichko, Y. S.; Olvera De La Cruz, M.; Stupp, S. I. *Philos. Trans. R. Soc. A* **2007**, *365*, 1417–1433.
2. (a) Korgel, B. A. *Science* **2005**, *309*, 1683–1684; (b) Fonseca, A. F.; Malta, C. P.; Galvão, D. S. *Nanotechnology* **2007**, *18*, 435606 (6pp); (c) Elias, A. L.; Harris, K. D.; Bastiaansen, C. W. M.; Broer, D. J.; Brett, M. J. *J. Micromech. Microeng.* **2005**, *15*, 49–54.
3. (a) Li, L.-S.; Jiang, H.; Messmore, B. W.; Bull, S. R.; Stupp, S. I. *Angew. Chem., Int. Ed.* **2007**, *46*, 5873–5876; (b) Engelkamp, H.; Middelbeek, S.; Nolte, R. J. M. *Science* **1999**, *284*, 785–788; (c) Kajitani, T.; Okoshi, K.; Sakurai, S.-I.; Kumaki, J.; Yashima, E. *J. Am. Chem. Soc.* **2006**, *128*, 708–709; (d) Iwaura, R.; Shimizu, T. *Angew. Chem., Int. Ed.* **2006**, *45*, 4601–4604; (e) George, S. J.; Ajayaghosh, A.; Jonkheijm, P.; Schenning, A. P. H. J.; Meijer, E. W. *Angew. Chem., Int. Ed.* **2004**, *43*, 3422–3425.
4. (a) Sone, E. D.; Zubarev, E. R.; Stupp, S. I. *Angew. Chem., Int. Ed.* **2002**, *41*, 1705–1709; (b) Hartgerink, J. D.; Zubarev, E. R.; Stupp, S. I. *Curr. Opin. Solid State Mater. Sci.* **2001**, *5*, 355–361; (c) Messmore, B. W.; Hulvat, J. F.; Sone, E. D.; Stupp, S. I. *J. Am. Chem. Soc.* **2004**, *126*, 14452–14458; (d) Messmore, B. W.; Stupp, S. I. *J. Am. Chem. Soc.* **2005**, *127*, 7992–7993; (e) Oda, R.; Huc, I.; Schmutz, M.; Candau, S. J.; MacKintosh, F. C. *Nature* **1999**, *399*, 566–569; (f) Sumiyoshi, T.; Nishimura, K.; Nakano, M.; Handa, T.; Miwa, Y.; Tomioka, K. *J. Am. Chem. Soc.* **2003**, *125*, 12137–12142; (g) Douliez, J.-P.; Navailles, L.; Nallet, F.; Gaillard, C. *ChemPhysChem* **2008**, *9*, 74–77.
5. (a) Shimizu, T.; Masuda, M.; Minamikawa, H. *Chem. Rev.* **2005**, *105*, 1401–1443; (b) Hill, J. P.; Jin, W.; Kosaka, A.; Fukushima, T.; Ichihara, H.; Shimomura, T.; Ito, K.; Hashizume, T.; Ishii, N.; Aida, T. *Science* **2004**, *304*, 1481–1483; (c) Lee, S. J.; Kim, E.; Seo, M. L.; Do, Y.; Lee, Y.-A.; Lee, S. S.; Jung, J. H.; Kogiso, M.; Shimizu, T. *Tetrahedron* **2008**, *64*, 1301–1308.
6. (a) Jiménez, J. L.; Nettleton, E. J.; Bouchard, M.; Robinson, C. V.; Dobson, C. M.; Saibil, H. R. *Proc. Natl. Acad. Sci. U.S.A.* **2002**, *99*, 9196–9201; (b) Serpell, L. C.; Sunde, M.; Benson, M. D.; Tennent, G. A.; Pepys, M. B.; Fraser, P. E. *J. Mol. Biol.* **2000**, *300*, 1033–1039; (c) Knowles, T. P.; Fitzpatrick, A. W.; Meehan, S.; Mott, H. R.; Vendruscolo, M.; Dobson, C. M.; Welland, M. E. *Science* **2007**, *318*, 1900–1903.
7. (a) Chothia, C. *J. Mol. Biol.* **1973**, *75*, 295–302; (b) Shamovsky, I. L.; Ross, G. M.; Riopelle, R. J. *J. Phys. Chem. B* **2000**, *104*, 11296–11307; (c) Rubin, N.; Perugia, E.; Goldschmidt, M.; Fridkin, M.; Addadi, L. *J. Am. Chem. Soc.* **2008**, *130*, 4602–4603.
8. Sunde, M.; Serpell, L. C.; Bartlam, M.; Fraser, P. E.; Pepys, M. B.; Blake, C. C. F. *J. Mol. Biol.* **1997**, *273*, 729–739.
9. (a) Hartgerink, J. D.; Beniash, E.; Stupp, S. I. *Science* **2001**, *294*, 1684–1688; (b) Silva, G. A.; Czeisler, C.; Niece, K. L.; Beniash, E.; Kessler, J. A.; Harrington, D. A.; Stupp, S. I. *Science* **2004**, *302*, 1352–1355; (c) Mart, R. J.; Osborne, R. D.; Stevens, M. M.; Ulijn, R. V. *Soft Matter* **2006**, *2*, 822–835; (d) Behanna, H. A.; Donners, J. J. J. M.; Gordon, A. C.; Stupp, S. I. *J. Am. Chem. Soc.* **2005**, *127*, 1193–1200.
10. (a) Velichko, Y. S.; Stupp, S. I.; Olvera De La Crux, M. *J. Phys. Chem. B* **2008**, *112*, 2326–2334; (b) Jiang, H.; Guler, M. O.; Stupp, S. I. *Soft Matter* **2007**, *3*, 454–462; (c) Nowak, A. P.; Breedveld, V.; Pakstis, L.; Ozbas, B.; Pine, D. J.; Pochan, D.; Deming, T. J. *Nature* **2002**, *417*, 424–428; (d) Colombo, G.; Soto, P.; Gazit, E. *Trends Biotechnol.* **2007**, *25*, 211–218; (e) Hentschel, J.; Börner, H. G. *J. Am. Chem. Soc.* **2006**, *128*, 14142–14149.
11. (a) General, S.; Antonietti, M. *Angew. Chem., Int. Ed.* **2002**, *41*, 2957–2960; (b) Schlaad, H.; Antonietti, M. *Eur. Phys. J. E* **2003**, *10*, 17–23; (c) Yang, Z.; Liang, G.; Ma, M.; Gao, Y.; Xu, B. *J. Mater. Chem.* **2007**, *17*, 850–854.
12. Rowan, A. E.; Nolte, R. J. M. *Angew. Chem., Int. Ed.* **1999**, *37*, 63–68.
13. (a) Yamada, N.; Koyama, E.; Imai, T.; Matsubara, K.; Ishida, S. *Chem. Commun.* **1996**, *19*, 2297–2298; (b) Yamada, N.; Ariga, K.; Naito, M.; Matsubara, K.; Koyama, E. *J. Am. Chem. Soc.* **1998**, *120*, 12192–12199; (c) Ariga, K.; Kikuchi, J.-I.; Naito, M.; Yamada, N. *Polym. Adv. Technol.* **2000**, *11*, 856–864.
14. Kawano, S.-I.; Fujita, N.; Shinkai, S. *Chem.—Eur. J.* **2005**, *11*, 4735–4742.
15. Schenning, A. P. H. J.; Kilbinger, A. F. M.; Biscarini, F.; Cavallini, M.; Cooper, H. J.; Derrick, P. J.; Feast, W. J.; Lazzaroni, R.; Leclère, P.; McDonell, L. A.; Meijer, E. W.; Meskers, S. C. J. *J. Am. Chem. Soc.* **2002**, *124*, 1269–1275.
16. (a) Gesquière, A.; De Feyter, S.; De Schryver, F. C.; Schoonbeek, F.; van Esch, J.; Kellogg, R. M.; Feringa, B. L. *Nano Lett.* **2001**, *1*, 201–206; (b) Schoonbeek, F. S.; van Esch, J. H.; Wegewijs, B.; Rep, D. B. A.; de Haas, M. P.; Klapwijk, T. M.; Kellogg, R. M.; Feringa, B. L. *Angew. Chem., Int. Ed.* **1999**, *38*, 1393–1397.
17. Moore, J. S.; Stupp, S. I. *Macromolecules* **1990**, *23*, 65–70.
18. Fages, F.; Vögtle, F.; Žinić, M. *Top. Curr. Chem.* **2005**, *256*, 77–131.
19. Eyre, D. R. *Science* **1980**, *207*, 1315–1322.
20. (a) Rich, A.; Crick, F. H. C. *J. Mol. Biol.* **1961**, *3*, 483–506; (b) Kramer, R. Z.; Bella, J.; Brodsky, B.; Berman, H. M. *J. Mol. Biol.* **2001**, *311*, 131–147.
21. (a) Schlaad, H.; Krasia, T.; Antonietti, M. *J. Am. Chem. Soc.* **2004**, *126*, 11307–11310; (b) Böttcher, C.; Schade, B.; Ecker, C.; Rabe, J. P.; Shu, L.; Schlüter, A. D. *Chem.—Eur. J.* **2005**, *11*, 2923–2928.
22. Muraoka, T.; Cui, H.; Stupp, S. I. *J. Am. Chem. Soc.* **2008**, *130*, 2946–2947.
23. Toniolo, C.; Palumbo, M. *Biopolymers* **1977**, *16*, 219–224.
24. Becker, R. S.; de Melo, J. S.; Maçanita, A. L.; Elisei, E. *Pure Appl. Chem.* **1995**, *67*, 9–16.
25. (a) Graf, D. D.; Duan, R. G.; Campbell, J. P.; Miller, L. L.; Mann, K. R. *J. Am. Chem. Soc.* **1997**, *119*, 5888–5899; (b) Whitten, D. G. *Acc. Chem. Res.* **1993**, *26*, 502–509.
26. Harada, N.; Nakanishi, K. *Circular Dichroic Spectroscopy: Exciton Coupling in Organic Stereochemistry*; University Science Books: Mill Valley, CA, 1983.
27. (a) DiCésare, N.; Belletête, M.; Marrano, C.; Leclerc, M.; Durocher, G. *J. Phys. Chem. A* **1999**, *103*, 795–802; (b) Fujitsuka, M.; Cho, D. W.; Ohshita, J.; Kunai, A.; Majima, T. *J. Phys. Chem. C* **2007**, *111*, 1993–1998; (c) Hempenius, M. A.; Langeveld-Voss, B. M. W.; van Haare, J. A. E. H.; Janssen, R. A. J.; Sheiko, S. S.; Spatz, J. P.; Möller, M.; Meijer, E. W. *J. Am. Chem. Soc.* **1998**, *120*, 2798–2804.
28. Koga, T.; Matsuoka, M.; Higashi, N. *J. Am. Chem. Soc.* **2005**, *127*, 17596–17597.
29. (a) Cornelissen, J. J. L. M.; Donners, J. J. J. M.; de Gelder, R.; Graswinckel, W. S.; Metsellar, G. A.; Rowan, A. E.; Sommerdijk, N. A. J. M.; Nolte, R. J. M. *Science* **2001**, *293*, 676–680; (b) Metsellar, G. A.; Adams, P. J. H. M.; Nolte, R. J. M.; Cornelissen, J. J. L. M.; Rowan, A. E. *Chem.—Eur. J.* **2007**, *13*, 950–960.